Supporting information

Morphology of laser reduced films:

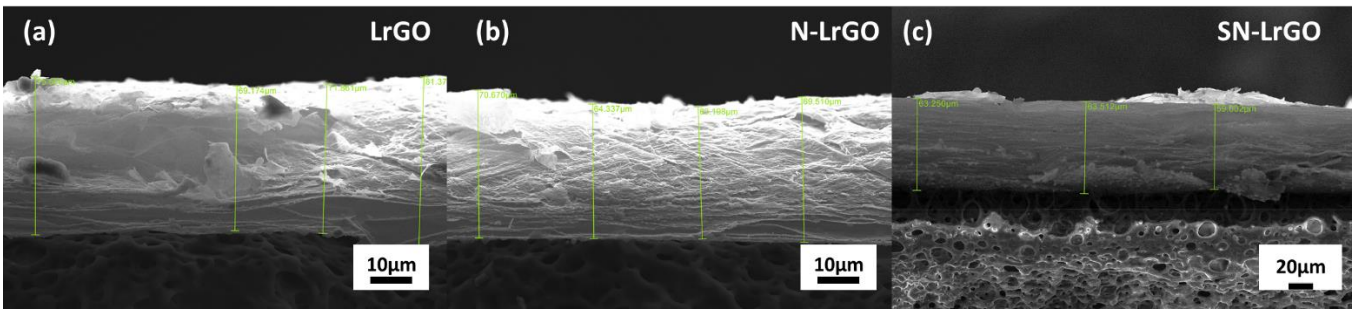

Fig. S1: SEM images of cross section area of; LrGO (a), N-LrGO (b), and SN-LrGO (c).

Structure of laser reduced films:

Table S1: Summary of Raman spectroscopy results

	LrGO	N-LrGO	SN-LrGO
D-band (cm^{-1})	1370	1343	1350
G-band (cm^{-1})	1582	1575	1580
2D-band (cm^{-1})	2700	2683	2695
$(FWHM)_G$ (cm^{-1})	122	38.98	28.25
$(FWHM)_{2D}$ (cm^{-1})	---	69	53.2
I_D/I_G	0.66	0.38	0.164
I_{2D}/I_G	0.018	0.82	0.87
L_D (nm)	15.9	22.8	32.87
$\boldsymbol{\eta_D}$ (cm^{-2})	2.26×10^{11}	1.1×10^{11}	5.23×10^{10}
$\boldsymbol{L_{sp^2}}$ (nm)	25.15	51.87	107

Electrical conductivity:

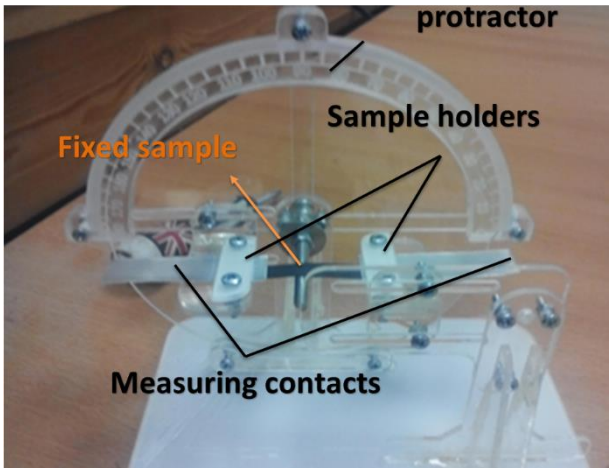

Fig. S2: Bending test rig consists of protractor, sample holders, and measuring contacts.

Electrochemical performance:

The volumetric and areal specific capacitances were calculated from GCD according to Equation (2) and (3), respectively:

$$C_v = \frac{I}{V(dI/dt)} \quad (2)$$

$$C_a = \frac{I}{A(dI/dt)} \quad (3)$$

where C_v (F cm^{-3}) is the volumetric specific capacitance, C_a (F cm^{-2}) is the aerial specific capacitance, I (A) is the constant charge-discharge current (A), dV/dt (V s^{-1}) is the slope of the discharge curve, V (cm^3) and A (cm^2) are the volume and the planar area of the planar SC device, respectively. The Energy density E (Wh cm^{-3}) and the power density P (W cm^{-3}) of the tested planar SC devices were calculated using Equation (3) and Equation (4), respectively:

$$E_V = \frac{C(\Delta E)^2}{2 \times 3600} \quad (4)$$

$$P_V = \frac{\Delta E}{4R_s V} \quad (5)$$

where ΔE (V) is the potential window, and the R_s (Ω) is the equivalent series resistance (ESR) and can be found from either EIS analysis.

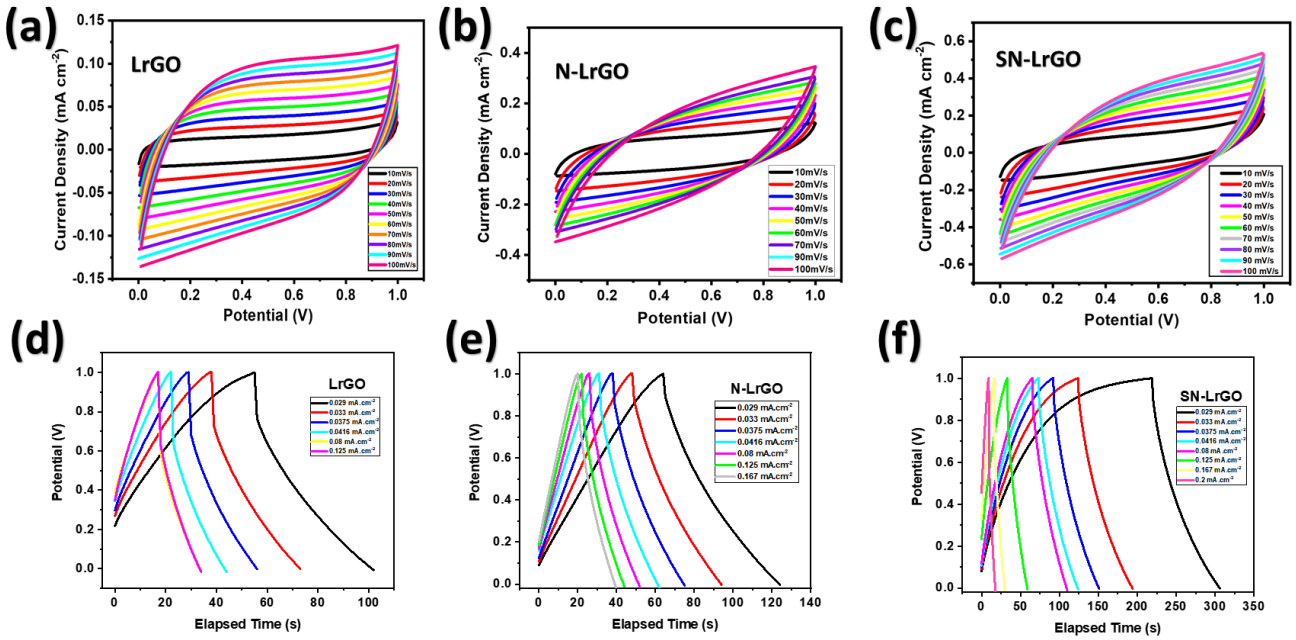

Figure S3: Cyclic voltammetry and GCCD curves of a) LrGO, b) N-LrGO, and c) SN-LrGO based planar SC.

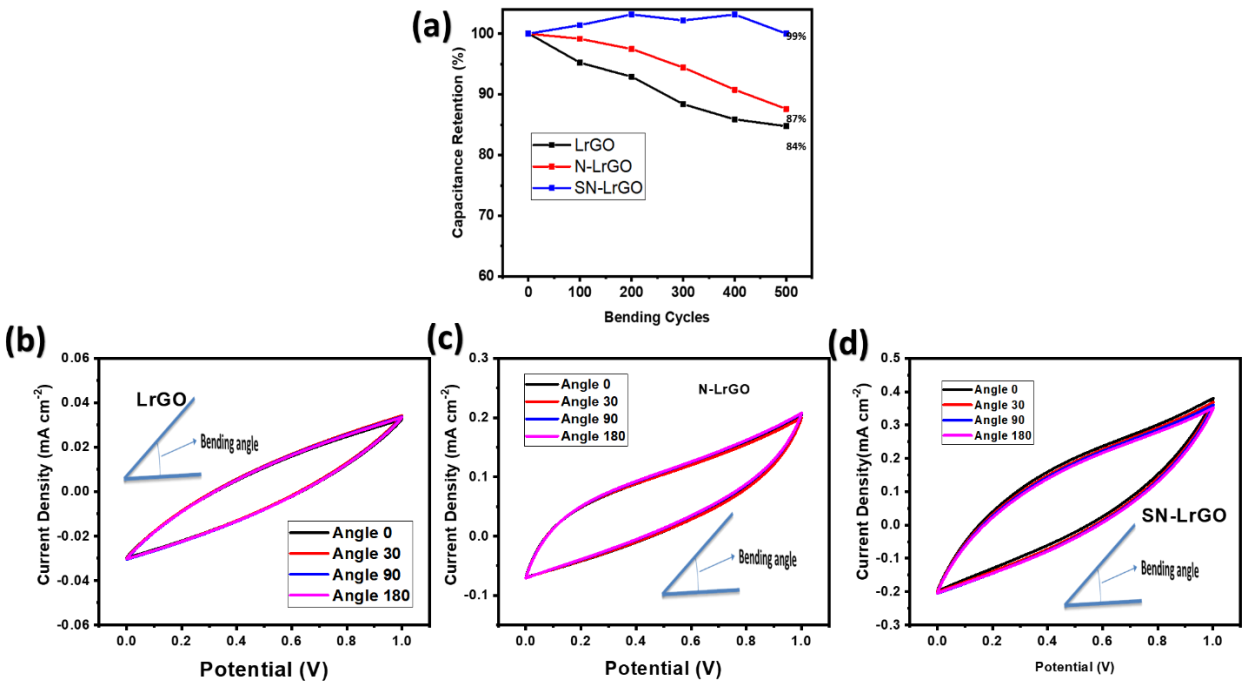

Fig. S4: Capacitance Retention up to 500 bending cycles at a bending angle of 180˚ (a); CV profiles at different bending angles 0˚, 30˚, 90˚, and 180˚ for LrGO (b), NrGO (c), and SN-LrGO (d) PSCs.

The capacitance retention of the SN-LrGO, N-LrGO, and LrGO PSCs was measured against bending cycles, **Fig. S3** After 500 bending cycles at angle of 180˚, the SN-LrGO PSC retained 99.2 of its initial capacitance measured at $10mVS^{-1}$. Also, the fabricated cells displayed almost no variation in the shapes of the CV curves measured at different bending angles 0˚, 30˚, 90˚, and 180˚, Fig. 9(b-d). Thus, SN-LrGO, N-LrGO and LrGO PSCs were able to maintain their superior capacitive and mechanical performance after multiple charging/discharging as well as severe and continual bending.

Table S2: Comparison of capacitance values of different micro-supercapacitors from literature.

Material	***Areal Capacitance (mF/cm^2)***	***Current density (mA/cm^3)***	***Interspacing (μm)***	***Energy density (mWh/cm^3)***	***Power density (W/cm^3)***	***Ref.***
Laser Scribed Graphene	*2.32 mF/cm^2*	*16.8 mA/cm^3*	*150 μm*	*0.25*	*14*	[1]
Laser Reduced Hydrated graphite oxide films	*0.51 mF/cm^2*	-	*0.5 mm*	*$4.3 \times 10^{-4} Wh/cm^3$*	*1.7*	[2]
Activated carbon (AC)	*1.1 mF/cm^2.*	*100mV/s*	*40 μm*	*15.9 mJ.cm-²*	-	[3]
Onion like carbon	*1.7 mF/cm^2*	*100mV/s*	*100 μm*	-	*1 kW cm^{-3}*	[4]
Graphene/CNT	*6.1 mF cm − 25.1 mF/cm^2*	*at 0.01 V s^{-1}*		*0.68 $mWhcm^{-3}$*	*77 Wcm $^{-3}$*	[5]
Graphene-CNT carpet	*2.16 mF/cm^2 in aqueous electrolytes 3.93 mF/cm^2in ionic liquids*	*0.5 A/cm^3*	-	*2.42 mWh/cm3*	*115 W/cm3*	[6]
vanadium disulfide nanosheets	4.76 mF/cm^2	*20-200 mV/s*	-	-	-	[7]
molybdenum disulfide	8 mF/cm^2	*0.22 A m^{-2}*	*200 μm*			[8]
Boron doped laser induced	16.5 mF/cm^2	*0.05 mA/cm2*	*300 μm*	0.56	*5 W/cm^3*	[9]
PANI/exfoliated graphene	1.5 mF cm^{-2}	*10 mV/s*	*100 μm*	1.06–6.67 mWh cm^{-3}	600 W cm^{-3}	[10]

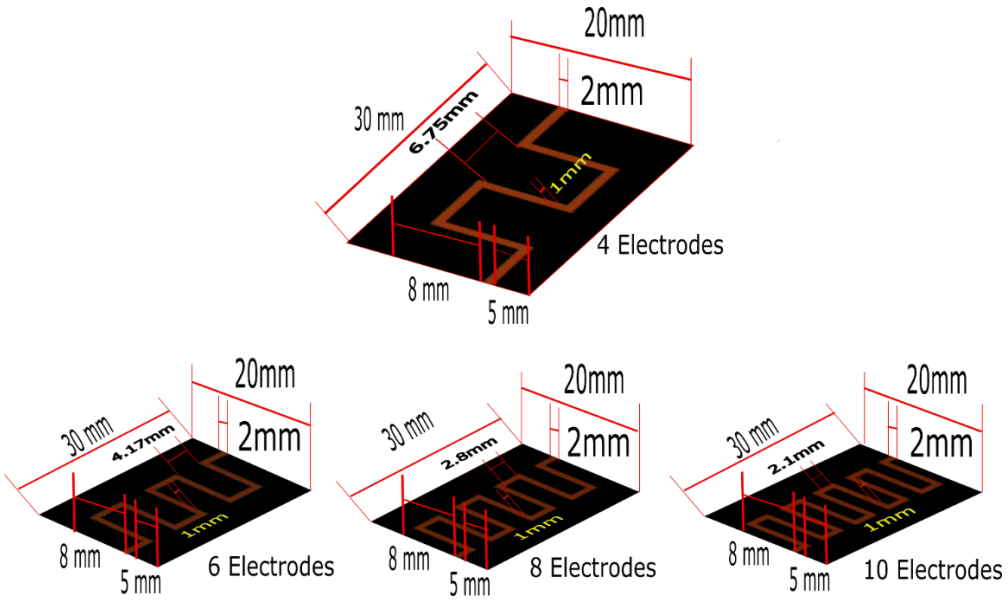

Fig. S5: Dimensions of planar devices with different number of interdigitated electrodes 4,6,8 and 10 electrodes.

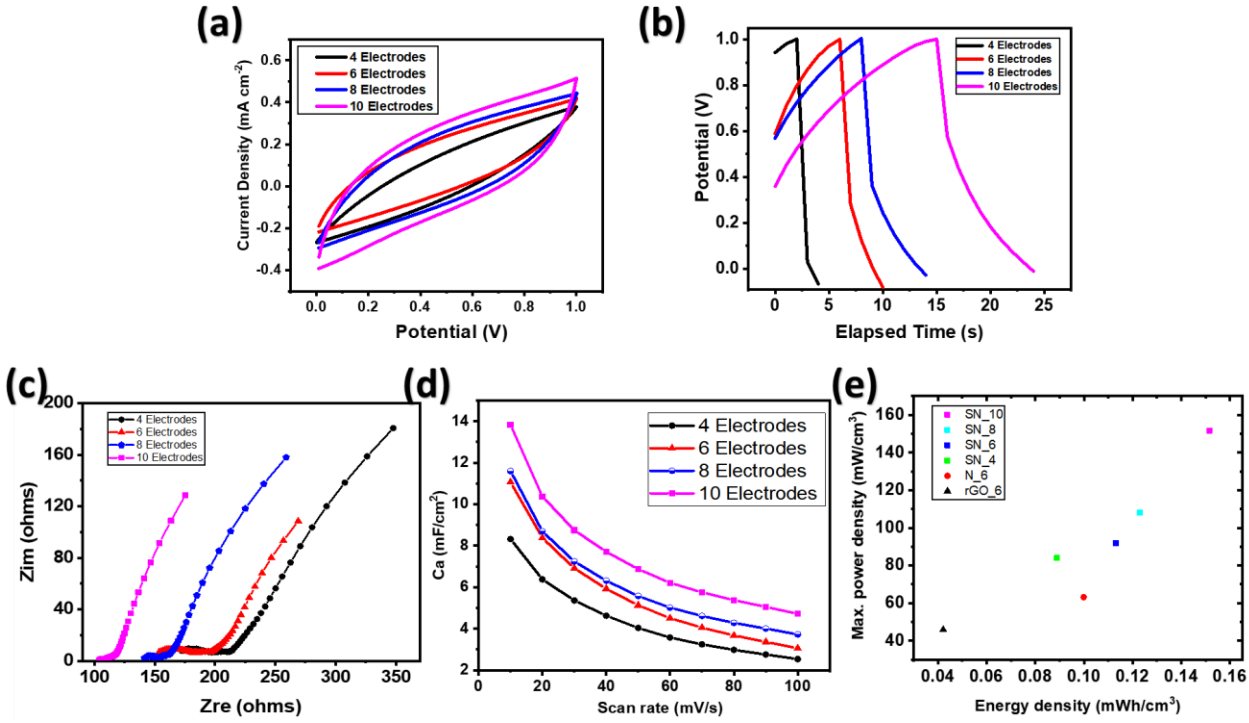

Fig. S6: Effect of number of interdigitated fingers in SN-LrGO PSC on; CV (a), GCD (b), C_a vs scan rate (c), EIS (d) and Maximum power density versus energy density of PSC cells.

Four interdigitated architectures composed of 4, 6, 8 and 10 electrodes were studied. The interspacing between these fingers was kept fixed at 1 mm, while the width of the fingers varies accordingly, **Fig. S4.** As seen in **Figs. S5 (a) and (b)**, increasing the number of fingers of interdigitated electrodes resulted in an increase in the enclosed area of the CV curve and the discharge time of the GCD profile. Along with a decrease in the IR drop of the GCD profile and, resistance related components (R_{ct} and R_{ESR}) derived from the Nyquist plots, **Fig. S5(c).** This confirms an increase in capacitance and a decrease in resistance of the PSC cell is observed by increasing the number of the interdigitated electrodes. Quantitatively, C_a calculated at 10 mV S^{-1} for the cell made of interdigitated SN-LrGO with 10 fingers, is 13.8 mF cm^{-2}, which translates to C_v value of 2195 mF cm^{-3}. These values are significantly higher than those of the cell with 4 fingers with C_a equals to 8.3mF cm^{-2} and C_v is1320 mF cm^{-3}, **Fig. S5(d)**. In return, the more interdigitation, the higher are the energy and power densities of the fabricated PSC cells, **Fig. S5(e).** The estimated volumetric power and energy densities of the SN-LrGO PSC cell is increased from 85 mW cm^{-3} at energy density of 0.093 mWh cm^{-3} to 151.7 mW cm^{-3} at energy density of 0.152 mWh cm^{-3} when the number of electrodes is increased from 4 to 10 respectively, see Table S3. This in turns increase the capacity per footprint area which is crucial key for the miniaturization of the energy storage devices in order to be more compliant with modern electronic applications. According to previous reports, increasing in the number of electrodes per footprint area typically enables a larger access area for the electrolyte along with a reduction in the average migration distance for the ions and an increase in the electron transfer dynamics [1,11].

Table S3: Summary of the electrochemical performance for the fabricated cells with different number of interdigitated fingers measured at 10mV S^{-1}.

PSC	**4 interdigitated fingers PSC**	**6 interdigitated fingers PSC**	**8 interdigitated fingers PSC**	**10 interdigitated fingers PSC**
C_a *(mF* cm^{-2}*)*	*8.31*	*11*	*11.6*	*13.8*
C_v *(mF* cm^{-3}*)*	*1320*	*1756*	*1841*	*2195*
E_V *(mWh* cm^{-3}*)*	0.183	0.24	0.256	0.30
P_{Vmax} *(mW* cm^{-3}*)*	83.93	91	*108*	*151.7*

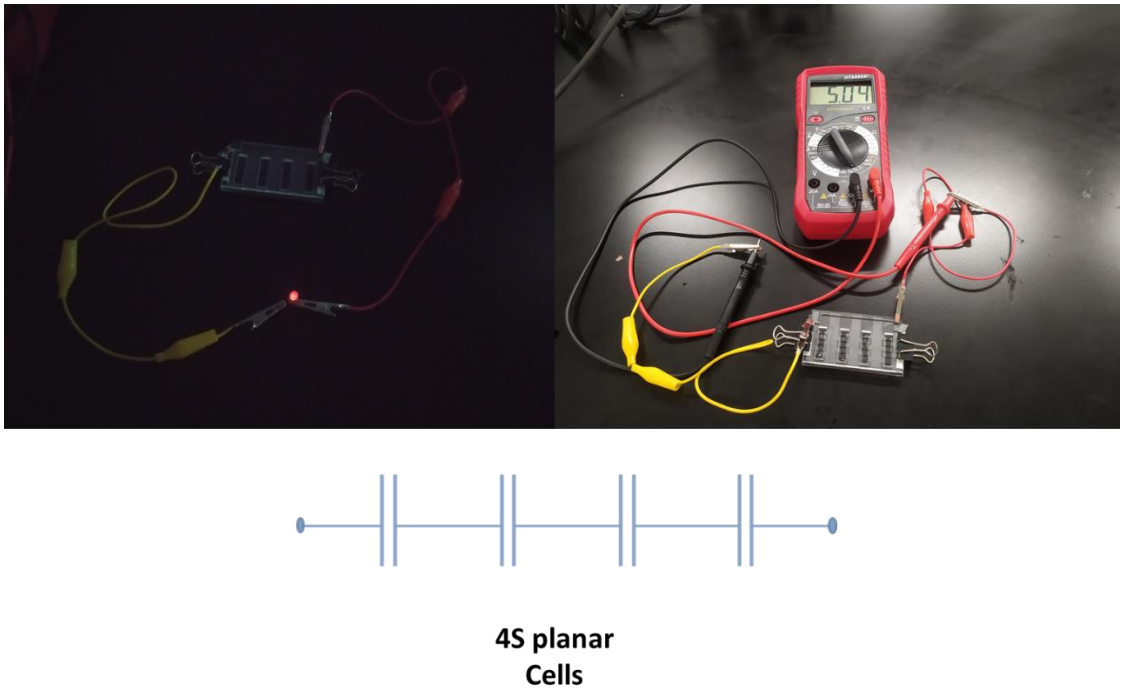

Fig. S7: An array composed of 4 series (4S) cells of PSCS is used to light a Red LED, potential window was increased up to 5 V.

References:

1. El-Kady, M. F.; Kaner, R. B. Scalable fabrication of high-power graphene micro-supercapacitors for flexible and on-chip energy storage. *Nat. Commun.* **2013**, *4*, 1475, doi:10.1038/ncomms2446.

2. Gao, W.; Singh, N.; Song, L.; Liu, Z.; Reddy, A. L. M.; Ci, L.; Vajtai, R.; Zhang, Q.; Wei, B.; Ajayan, P. M. Direct laser writing of micro-supercapacitors on hydrated graphite oxide films. *Nat. Nanotechnol.* **2011**, *6*, 496–500, doi:10.1038/nnano.2011.110.

3. Pech, D.; Brunet, M.; Taberna, P.; Simon, P.; Fabre, N.; Mesnilgrente, F.; Conédéra, V.; Durou, H. Elaboration of a microstructured inkjet-printed carbon electrochemical capacitor. *J. Power Sources* **2010**, *195*, 1266–1269, doi:10.1016/j.jpowsour.2009.08.085.

4. Pech, D.; Brunet, M.; Durou, H.; Huang, P.; Mochalin, V.; Gogotsi, Y.; Taberna, P.-L.; Simon, P. Ultrahigh-power micrometre-sized supercapacitors based on onion-like carbon. *Nat. Nanotechnol.* **2010**, *5*, 651–654, doi:10.1038/nnano.2010.162.

5. Beidaghi, M.; Wang, C. Micro-Supercapacitors Based on Interdigital Electrodes of Reduced Graphene Oxide and Carbon Nanotube Composites with Ultrahigh Power Handling Performance. *Adv. Funct. Mater.* **2012**, *22*, 4501–4510, doi:10.1002/adfm.201201292.

6. Lin, J.; Zhang, C.; Yan, Z.; Zhu, Y.; Peng, Z.; Hauge, R. H.; Natelson, D.; Tour, J. M. 3‐Dimensional Graphene Carbon Nanotube Carpet-Based Microsupercapacitors with High Electrochemical Performance. *Nano Lett.* **2013**, *13*, 72–78, doi:10.1021/nl3034976.

7. Feng, J.; Sun, X.; Wu, C.; Peng, L.; Lin, C.; Hu, S.; Yang, J. Metallic Few-Layered VS 2 Ultrathin Nanosheets : High Two-Dimensional Conductivity for In-Plane Supercapacitors. *J. Am. Chem. Soc.* **2011**, *133*, 17832–17838, doi:10.1021/ja207176c.

8. Cao, L.; Yang, S.; Gao, W.; Liu, Z.; Gong, Y.; Ma, L.; Shi, G.; Lei, S.; Zhang, Y.; Zhang, S.; Vajtai, R. Direct Laser-Patterned Micro-Supercapacitors from Paintable MoS 2 Films. *Small* **2013**, *9*, 2905–2910, doi:10.1002/smll.201203164.

9. Peng, Z.; Ye, R.; Mann, J. A.; Zakhidov, D.; Li, Y.; Smalley, P. R.; Lin, J.; Tour, J. M. Flexible Boron-Doped Laser-Induced Graphene Microsupercapacitors. *ACS Nano* **2015**, *9*, 5868–5875, doi:10.1021/acsnano.5b00436.

10. Liu, Z.; Liu, S.; Dong, R.; Yang, S.; Lu, H.; Narita, A.; Feng, X.; Müllen, K. High Power In-Plane Micro-Supercapacitors Based on Mesoporous Polyaniline Patterned Graphene. *Small* **2017**, *13*, 1–5, doi:10.1002/smll.201603388.

12. Ghoniem, E.; Mori, S.; Abdel-Moniem, A. Low-cost flexible supercapacitors based on laser reduced graphene oxide supported on polyethylene terephthalate substrate. *J. Power Sources* **2016**, *324*, 272–281, doi:10.1016/j.jpowsour.2016.05.069